

**United States
Department of
Agriculture**

**Natural
Resources
Conservation
Service**

**c/o USDA Forest Service
11 Campus Boulevard
Suite 200
Newtown Square, PA 19073
(610) 557-4233; FAX: (610) 557-4200**

Subject: SOI – Ground-penetrating radar (GPR) study of ice-wedge networks
at Barrow, Alaska

Date: 4 May 2006

To: Robert N. Jones
State Conservationists
USDA-Natural Resources Conservation Service
800 West Evergreen, Suite 100
Palmer, AK 99645-6546

Dr. Fredrick E. Nelson
Department of Geography
University of Delaware
207 Pearson Hall
Newark, DE 19716

Dr. Ken Hinkel
Department of Geography
University of Cincinnati
400F Braunstein
Cincinnati, OH 45221-0131

Participants:

Jim Doolittle, Research Soil Scientist, USDA-NRCS-NSSC, Newtown Square, PA
Benjamin Jones, Environmental Scientist, Science Applications International Corporation (SAIC), Anchorage, AK
Mikhail Z. Kanevsky, Post Doctoral Fellow, University of Alaska Fairbanks, Fairbanks, AK
John Kimble, Retired Research Soil Scientist, USDA-NRCS-NSSC, Lincoln, NE
Ken Hinkel, Professor, Geography Department, University of Cincinnati, Cincinnati, OH
Fritz Nelson, Professor, Geography Department, University of Delaware, Newark, DE
Jeffrey Munroe, Assistant Professor, Geology Department, Middlebury College, Middlebury, VT

Activities:

All field activities were completed on 17 to 22 April 2006.

Summary:

This study represents the first known attempt to use ground-penetrating radar (GPR) and three-dimensional (3D) radar imagery to map the subsurface structure and geometry of ice-wedge polygons. In this study, 3D imaging techniques helped to reduce interpretation uncertainties and to identify the subsurface geometry of ice-wedges networks. These graphic displays greatly improved the quality of radar interpretations. Time-slice images effectively showed the geometry and trends of ice-wedge networks that were not evident on conventional two-dimensional (2D) radar records. Compared with 2D radar interpretations of ice wedges and ice-wedge networks, 3D data interpretations are more complete and less ambiguous.

The spacing of radar traverse lines used to construct 3D images was too wide (50 cm) to prevent spatial aliasing and did result in some reduction in the resolution of GPR data. However, this spacing is acceptable as it did provide useful information concerning the subsurface structure and geometry of ice-wedge networks.

A GPR survey of a late 1960s research site revealed the general location of shallowly buried, 1 cm diameter, copper tubing. While the general orientation of the buried tubing within the site could be discerned in both 2D radar records and 3D radar

images, the location and continuity of individual weaves of tubing were ambiguous. Spatial variations in snow depths appearing on radar records confirmed that the copper tubing is buried in a slight depression, which is overlain by deeper columns of snow.

With kind regards,

James A. Doolittle
Research Soil Scientist
National Soil Survey Center

cc:

- B. Ahrens, Director, National Soil Survey Center, USDA-NRCS, Federal Building, Room 152, 100 Centennial Mall North, Lincoln, NE 68508-3866
- M. Golden, Director, Soil Survey Division, USDA-NRCS, Room 4250 South Building, 14th & Independence Ave. SW, Washington, DC 20250
- D. Hammer, National Leader, Soil Survey Investigations, National Soil Survey Center, USDA-NRCS, Federal Building, Room 152, 100 Centennial Mall North, Lincoln, NE 68508-3866
- J. Moore, State Soil Scientist/MLRA Office Leader, USDA-NRCS, 800 West Evergreen, Suite 100, Palmer, AK 99645-6546
- W. Tuttle, Soil Scientist (Geophysical), USDA-NRCS-NSSC, P.O. Box 60, 207 West Main Street, Rm. G-08, Federal Building, Wilkesboro, NC 28697

Background:

Ice-wedge polygons are distinct micro-features on the Arctic Coastal Plain of Alaska. Here, slightly raised polygons are separated by troughs containing ice wedges. Ice wedges (see Figure 1) are vertically orientated masses of foliated ice that form in perennial frozen ground (Brown, 1967). Characteristically, ice wedges are downward narrowing and range from 1 to 300 cm in width and 1 to 10 m in depth (Price, 1972). Extremely cold soil temperatures and thermal contraction are factors responsible for the development of ice wedges. Ice wedges result from the annual filling of thermal contraction cracks with hoar-frost or snow melt waters (Brown, 1967). In the summer, the permafrost expands causing horizontal compression and the displacement of surrounding soil materials (Price, 1972). The compression and displacement of soil materials forms low polygonal mounds and intervening troughs. In the winter, renewed thermal contraction occurs in the zone of weakness formed by the ice wedge (Price, 1972). Through this repeated cycle, the ice wedge grows. As the ice wedge grows, adjoining soils are subjected to compaction and displacement, troughs develop over ice wedges, and extensive honeycomb systems of ice-wedge polygons are formed (see Figure 2).



Figure 1. An ice-wedge (photograph courtesy of Ben Jones).

A network of ice-wedge networks produces ice-wedge polygons. In the Barrow area, about 65 % of the surface is covered by polygonal ground (Brown, 1967). The ice-wedge networks often display orthogonal junctions with straight line tracks that are up to several hundreds of meters in length (Mangold et al., 2005). The diameter of ice-wedge polygons varies from a few to over 100 m and is dependent upon the age and spacing of ice wedges (Price, 1972). Depending on the relative elevation of the polygon's center and margins, ice-wedge polygons are described as low- or high-centered. Relief of ice-wedge polygons is about 15 to 45 cm (Hussey and Michelson, 1966).

The purpose of this investigation was to use ground-penetrating radar (GPR) to investigate the subsurface structure and configuration of ice-wedge networks near Barrow, Alaska.

Ground-Penetrating Radar:

Ground-penetrating radar (GPR) is specifically designed for shallow subsurface investigations. A positive feature of GPR is its ability to quickly and easily provide high-resolution images of the subsurface, which aids the lateral extension of information obtained at coring sites. Frozen ground has electrical properties that are favorable to GPR. Scott and other (1990) observed that as the soil temperature drops below 0°C, the electrical conductivity, dielectric permittivity, and loss tangent decrease. As water freezes in soils, radar penetration depth increases. However, as the amount of ice increases, the

contrast in electromagnetic properties between frozen soil layers decreases and the detection of some soil and stratigraphic features with GPR is obscured.



Figure 2. Ice-wedge polygons, a form of patterned ground, are conspicuous landforms in the Barrow area (photograph courtesy of Ben Jones).

Ground-penetrating radar has been used extensively in areas of permafrost. Ground-penetrating radar has been used to study spatial and temporal variations in the thickness of the active layer and the permafrost table (Wong et al., 1977; Annan and Davis 1978; Pilon et al., 1979, 1985; Doolittle et al., 1990, 1992; Moorman et al., 2003; Wu et al., 2005). In addition, GPR has been used to measure the relative dielectric permittivity of frozen sediments (Annan et al., 1975; Annan and Davis, 1976; Davis et al., 1976; Arcone et al., 1982; Arcone and Delaney 1982, 1984, 1989). It has also been used to identify and map areas of massive ground ice (Kovacs and Morey, 1979, 1985; Arcone et al., 1982; Dallimore and Davis, 1987; Scott et al., 1990; Robinson et al., 1993), taliks (Arcone et al., 1998) and the internal structure and ice composition of pingos (Kovacs and Morey, 1985; Ross et al., 2005) and palsas (Sequin, 1986; Doolittle et al., 1992; Horvath, 1998). Although applications have been limited (Vonder Mühl et al., 2002) GPR has not been found to be suited to mapping mountain permafrost

Previous GPR study at Barrow (Hinkel et al., 2001) demonstrated that the most conspicuous subsurface reflectors observed in two-dimensional (2D) radar records obtained with a 400 MHz antenna were ice wedges. Ice wedges contrast in dielectric properties with the surrounding permafrost materials and often produce identifiable, high-amplitude hyperbolic reflections. In addition, because of the presence of an ice-rich layer at the base of the active layer, the long-term position of the permafrost table, though weakly expressed and often partially obscured by reflections from overlying soil interfaces, can be traced laterally across some radar records.

Cryoturbated soil horizons are difficult to distinguish on radar records. Cryoturbation results in the mixing of soil materials. As a result of cryoturbation, soil horizons are warped, discontinuous, and broken (Höfle et al., 1998). Because of their ice-rich, disrupted and mixed nature, most soil horizons lack sufficient contrast in dielectric properties or are too closely spaced to be evident with a 400 MHz antenna.

Three-dimensional GPR Images:

An emerging approach to GPR interpretations is the three-dimensional (3D) visualization of radar data. Recently, with the advent of digital GPR outputs, and the availability of more powerful computers and advanced data processing software, the

geometry and structure of subsurface features recorded on radar records can be analyzed from a three-dimensional perspective. Compared with single, two-dimensional (2D) GPR traverse information, 3D images can provide unparalleled resolution and detail of subsurface features (Grasmueck and Green, 1996) and help identify weakly expressed subsurface features and patterns.

Under favorable conditions, 3D imaging of radar data can facilitate the interpretation of spatial relationships and the analysis of structural and stratigraphic features. To construct 3D images, relatively small areas (5 to 50 m²) are intensively surveyed with closely spaced (typically 0.2 to 0.5 m), parallel GPR traverse lines. The relatively dense network of traverse lines is necessary to resolve the geometry and size of different subsurface features and to reduce spatially aliasing of the data (Grasmueck and Green, 1996). Data from these closely-spaced lines are processed into a 3D image. Once processed, arbitrary cross-sections, insets, and/or time slices can be extracted from the 3D data set. Three-dimensional imaging permits the rapid display of the data volume from different cross-sections and directions. Some software packages allow the observer to travel through the entire data volume with animated imagery (Grasmueck, 1996).

The acquisition of data for 3D images requires greater expenditures of time and effort than 2D images. Because of the time required to conduct fieldwork over limited areas and to process data, the use of 3D images has been restricted (Binningsbo et al., 2000). Three dimensional radar images have been extensively used in archaeological (Conyers and Goodman, 1997; Whiting et al., 2000; Grasmueck et al., 2004; Leucci and Negri, 2006) and infrastructure investigations (Sudarmo et al., 1996). Three-dimensional radar imaging has also been used to characterize sedimentary sequences and to better understand the internal structure and geometry of rocks (Asprion and Aigner, 1997, 2000; McMechan et al., 1997; Corbeau et al., 2001, 2002; Szerbiak et al., 2001; Grasmueck et al., 2004). Three-dimensional GPR images have been used to characterize the internal structure of glacial drift (Beres et al., 1995; Asprion and Aigner, 1999), faults (Demagnet et al., 2001; Green et al., 2003), and dunes (Jol et al., 2002; van Dam, 2002) and to map water tables (Lehmann and Green, 1999). In these investigations, the potentials of 3D imaging to characterize the structure and geometry of subsurface features were influenced by the soil environment, number of ground-truth observations, and existing knowledge of the study sites.

In recent years, a sophisticated type of GPR data manipulation, known as *amplitude slice-map analysis*, has been used in several investigations (Conyers and Goodman, 1997). In this analysis of GPR data, amplitude differences within the 3-D image are analyzed in "*time-slices*" that examine only changes within specific depth intervals in the ground (Conyers and Goodman, 1997). Time-slice data are created using spatially averaged amplitudes of return reflections. The reflected energy is averaged horizontally between each set of parallel radar records and in a specified time window to create a time-slice. Each amplitude time-slice shows the spatial distribution of reflected wave amplitudes, which are indicative of changes in soil properties or the presence of subsurface features.

Equipment:

The radar unit is the TerraSIRch Subsurface Interface Radar (SIR) System-3000, manufactured by Geophysical Survey Systems, Inc. (Salem, New Hampshire).¹ The SIR System-3000 weighs about 9 lbs (4.1 kg) and is backpack portable. With an antenna, this system requires two people to operate. As high resolution of relatively shallow subsurface features was required in this study, antennas with center frequencies of 400 and 900 MHz were used.

Radar records contained in this report were processed with the RADAN for Windows (version 5.0) software program (Geophysical Survey Systems, Inc., Salem, New Hampshire).¹ Processing included setting the initial pulse to time zero, color transformation, marker editing, distance normalization, migration, high pass horizontal filtration, and range gain adjustments. All radar records were migrated to remove hyperbola diffractions and to correct the geometry of inclined soil horizons and stratigraphic layers. For each site, radar records were processed into three-dimensional images using the 3D QuickDraw for RADAN Windows NT software (Geophysical Survey Systems, Inc., Salem, New Hampshire).¹ Once processed, 3D cubes, arbitrary cross sections, and time slices were viewed and selected images attached to this report.

Study Area:

The study areas are located near the village of Barrow, Alaska, at the northern extremity of the Arctic Coastal Plain physiographic unit (Wahrhaftig, 1965). Barrow has a cold maritime climate. The mean annual air temperature is about -12 °C (Hinkel et al., 2003). Mean annual precipitation is 106 mm, with about 63% falling as rain during the months of July through September (Hinkel et al., 2003). The area is underlain by continuous permafrost. At Barrow, the thickness of permafrost is greater than 400 meters (Hinkel et al., 2003). The depth of maximum seasonal thaw (active layer) varies from about 30 to 90 cm (Hinkel and Nelson, 2003).

¹ Manufacturer's names are provided for specific information; use does not constitute endorsement.

The Arctic Coastal Plain is characterized by multiple thaw lakes that are elongated in a north-northwesterly direction (Ping et al., 2004). Organic layers are thickest in the bottoms of thaw lakes (Höefle et al., 1998). Low-centered polygons are common on younger thaw lake surfaces while high-centered polygons dominate older thaw lake surfaces (Ping et al., 2004). The centers of low-centered polygons are nearly level and poorly or very poorly drained (Ping et al., 2004). Typic Aquorthels dominated the centers of low-centered polygons (Höefle et al., 1998). Troughs are dominated by Glacis Aquorthels (Höefle et al., 1998). Soils on slightly higher, convex rims of low-centered polygons are classified as Aquic Molliturbels or Typic Histoturbels (Ping et al., 2004). Soils in the centers of high-centered polygons are typically classified as Typic Historthels (Ping et al., 2004). On better drained, high-centered polygons, soils are typically classified as Aquic Molliturbels or Ruptic-Histic Aquiturbels (Bockheim et al., 1998; Ping et al., 2004).

Soils within the Barrow area contain about 50 to 75 percent segregated ice by volume in the upper two meters (Sellmann et al., 1975). This ice occurs in pores, lenses, massive layers and large ice wedges. Finer ice lenses often occur in the upper part of the mineral soil profile as a result of the relatively rapid freezing of water from the top down (Brown, 1967). In the lower part of mineral soils, thick (5 to 10 cm) horizontal ice lenses develop as a result of the migration and freezing of soil water from the permafrost table up (Brown, 1967). Ice lenses, ice nets and ataxitic ground ice fabrics are concentrated at the base of the active layer (Höefle et al., 1998).

Field Methods:

Because a thawed active layer is highly attenuating to radar energy, fieldwork was carried out in mid-April, when the active layer was still frozen. During summer months, adsorptive losses (high moisture contents) within thawed active layer and reflective losses (variable ice and water contents) within the upper part of the permafrost rapidly attenuate the radar energy and severely restrict penetration depths. Radar signals suffered less attenuation where the active layer is thin or nonexistent, and permafrost is very close to the soil surface (Lawson et al., 1998). In thawed, medium and fine textured sediments, radar signals are severely attenuated and little penetration is achieved (Arcone and Delaney, 1984).

At the time of this investigation, the study sites were blanketed with a mantle of snow that averaged about 30 cm and ranged from 0 to 70 cm thick. While snow cover provided easy access by snowmobiles with GPR and coring equipment to the study sites, its variable thickness within sites affected the accuracy of depth interpretations. While this study was being carried out, daytime temperatures ranged from about -27 to -3 ° F.

Survey grids were established at each site. To expedite GPR field work, two equal length and parallel lines were established across each site. At each site, the lengths of these two parallel lines were equal to the distance separating them. The two parallel lines defined a square grid area. Along each of these lines, survey flags were inserted in the ground at a constant interval of either 25 or 50 cm. For positional accuracy, GPR traverses were completed along a reference line, which was tightly stretched and sequentially moved between similarly numbered flags on the two parallel grid lines. Along the reference line, marks were spaced at 100 cm intervals. As the antenna was towed passed each reference mark, a vertical mark was impressed on the radar record. Walking, in a back and forth manner, along the reference line, which was moved sequentially between similarly numbered flags on the two parallel lines, completed a GPR grid survey.

With the exception of Grid Site 2, surveys were completed with a 400 MHz antenna. A 900 MHz antenna was used at Grid Site 2. In 3D surveys, traverse lines should be closely spaced so that data from individual lines overlap. However, because of often limited resources this is seldom accomplished. With the exception of Grid Site 2, the distance between individual traverse lines was 50 cm. At Grid Site 2, the distance was 25 cm.

Grid Site 1 was located on an old thaw lake basin. The site contains well-developed frost boils. Frost boils are 1 to 2 m in diameter. The flats between the frost boils contain well-defined ice-wedge troughs which are generally less than 50 cm deep and 75 to 150 cm wide. A 30 m² grid was set up across this site. The origin of this grid was located in its southeast corner.

Grid Site 2 was located at a 1960s research site of Dr. Jerry Brown. Copper tubing had been weaves in a back and forth manner across this small research site. The tubing is about 1 cm in diameter. The rows of tubing were spaced about 30 cm apart and buried at depths of about 15 to 20 cm. Over time, frost heave has displaced the tubing. The site was covered by a 10² m grid. The origin of the grid was located in the northeast corner of the site.

Grid Site 3 was located on the southern end of Foot Print Lake. Foot Print Lake is a drained thaw-lake basin. The basin was artificially drained in the early 1950s. During summer months, water ponds across this basin. The site has scattered low frost mounds. Thin layers of organic materials and silt-enriched lake sediments overly the basin. The site was covered by a 40² m grid. The origin of the grid was located in the southeast corner of the site.

Grid Site 4 is located on the Peterson Erosional Remnant. Based on radiometric dating, the Peterson Erosional Remnant is the oldest (9000 BP) surface presently recognized in this area. Other surfaces have been dated to as late as 5500 BP. The Peterson Erosional Remnant contains numerous small-scale, ice-wedge polygons. These high centered polygons are 2 to 3 m in diameter and generally less than 1 m in height. The site was covered by a 30² m grid. The origin of the grid was located in the northwest corner of the site.

Calibration:

Ground-penetrating radar is a time scaled system. This system measures the time that it takes electromagnetic energy to travel from an antenna to an interface (i.e., soil horizon, stratigraphic layer) and back. The relative dielectric permittivity (Er) is used to determine the velocity of signal propagation (v) according to the equation (Daniels, 2004):

$$\sqrt{Er} = c/v \quad [1]$$

In this equation, c represents the velocity of light in a vacuum (2.998 m/ns). The Er can range from 1 (air) to 80 (water).

The relationships among depth (d), two-way, pulse travel time (t) and velocity of propagation (v), are described in the following equation (Daniels, 2004):

$$d = vt/2 \quad [2]$$

Typical values for the Er and v of earthen materials found at Barrow are listed in Table 1. Arcone and Delaney (1989) estimated the Er of alluvial permafrost on the north slope of Alaska to range between 4.5 and 5. However, a lower Er is expected in more ice-rich materials. In alluvial deposits with high volumetric ice content (about 73 %), the Er was estimated to be 3.7 (Delaney and Arcone, 1984). In a GPR investigation conducted at Barrow in early May of 1999 (Hinkel et al., 2001), based on the depths to known reflectors observed in seven cores, the Er averaged 5.2 with a range of 3.4 to 7.7 for the upper 1 m of the soil profile. An Er of 5.2 (v = 0.13 m/ns) was used in the present investigation. High spatial variations in snow thickness, ice contents and soil materials were known to exist across each grid site. As variations these parameters will introduce errors into depth calculations, depth estimates used in this report should be viewed as approximations.

Table 1
Referenced relative dielectric permittivity (Er) and propagation velocity (v)
for materials encountered at Barrow, Alaska.

Material	Er	v	Source
Ice	3 to 4	0.150 to 0.173 m/ns	Conyers and Goodman, 1997
Permafrost	4 to 8	0.150 to 0.106 m/ns	Daniels et al., 2004
Snow	6 to 12	0.122 to 0.087 m/ns	Daniels et al., 2004

Interpretation of Radar Profiles:

Grid Site 1:

Grid Site 1 was located on an old thaw lake basin that contains well-developed frost boils. In general, radar records from this site were considered of poor interpretative quality and provided little information concerning the locations of ice-wedges or the geometry of ice-wedge networks. The snow depth was generally less than 30 cm across this site. Because of the thinness of the snow, the snow/soil interface was hardly discernible from the strong surface pulse on radar records.

Figure 3 is a representative portion of the radar record from this site (line Y = 27 m). The horizontal scale represents units of distance and is expressed in meters. The short, white, vertical lines at the top of the radar record represent the equally-spaced, flagged reference points. The depth scale is in meters and is based on an assumed constant propagation velocity of 0.13 m/ns.

In Figure 3, a green line has been used to highlight the snow/soil interface. In the upper part of this radar record are two distinguishable sets of bands: a higher amplitude set occurring at a depth of about 50 cm, and a lower amplitude set at a depth of about 75 cm (This radar record was not processed with a horizontal high pass filter to remove horizontal bands of noise and images). The identities of these sets of bands were not assessed during field work. One set may represent the permafrost table. However, as these bands are similar in appearance, occur at a comparable time (depth) interval (about 25 cm), and decrease in amplitude with increasing depth, they may also represent reverberations of the reflected signals from the snow/soil interface.

In Figure 3, a green-colored ellipse has been used to highlight an anomalous feature that is observable below the 27 m reference mark. The soil was cored at this location. Coring revealed an active frost boil with *ataxitic* cryogenic fabric occurring at a depth of 82 to 111 cm (maximum depth of coring). *Ataxitic* fabric is very ice-rich with soil aggregates appearing to be suspended in the ice (Ping et al., 2004). The high ice content of this *ataxitic* fabric is assumed to be responsible for the high-amplitude reflections and reverberations that led us to this site. On other radar records, sporadic patterns of reverberated signals from point reflectors suggest the locations of more *ataxitic* fabric, ice wedges, or buried artifact (the area has been repeatedly studied and several wire flags were observed during survey operations).

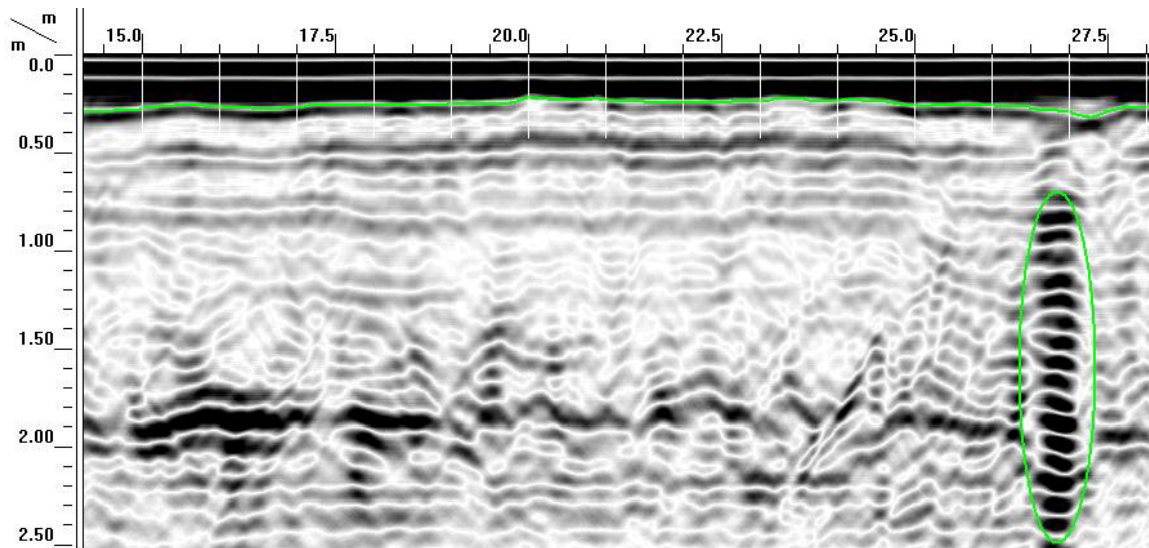


Figure 3. A representative radar record that was collected with a 400 MHz antenna along grid line 27 at Grid Site #1. The snow/soil interface and an area of *ataxitic* cryostructure have been highlighted by a green line and ellipse, respectively.

Figure 4 contains three time-slice images of the subsurface within Grid Site 1. All scales are in meters. For display purposes, the vertical scale of the cube has been highly exaggerated. The grid origin is located in the southeast corner of each time-slice image. The X axis is in the right foreground, the Y axis is in the left foreground. Assuming a constant signal propagation velocity of 0.13 m/ns, horizontal “time slices” were made across the imaged cube at depths of 0, 50 and 100 cm (propagation times of 0, 7.9, and 15.7 ns). Because the velocity of propagation varies across the grid area and with depth, these horizontal time-slices should be considered as only approximated depth slices. For each time-slice map, the thickness of the slice is 4 ns and the maximum reflected wave amplitude method has been used. Amplitude changes can be related to changes in soil properties and the locations of subsurface features.

In Figure 4, on the “0 cm” slice, areas of red amplitudes generally conform to areas of barren ground or thin snow cover. Areas of blue amplitudes are associated with deeper snow mantles. On the “50 cm” slice, areas of high amplitude red reflections are believed to represent the snow/soil interface which has been intercepted by the slice along lower-lying, ice-wedge troughs. In the “100 cm” slice, linear bands of high amplitude red reflections that are orientated parallel with the X axis represent background and system noise. The lines of high amplitude red reflections that extend along the Y axis and occur at the 0 and 30 m marks along the X axis (edges of grid area) represent interference from the metallic survey flags that were placed too close to the margins of the survey grid area. The line of high amplitude red reflections that parallels the Y axis and occur at X axis 19 m is orthogonal to the direction of radar traverses and is assumed to represent a buried utility line (site was instrumented).

Other than isolated frost boils or ice wedges, radar records from Grid Site 1 were nondescript. At this site, the use of advanced processing and display techniques did not improve interpretations or the information that was gathered with unprocessed, 2D radar records. Results from the survey at Grid Site 1 represent an unsuccessful GPR field study.

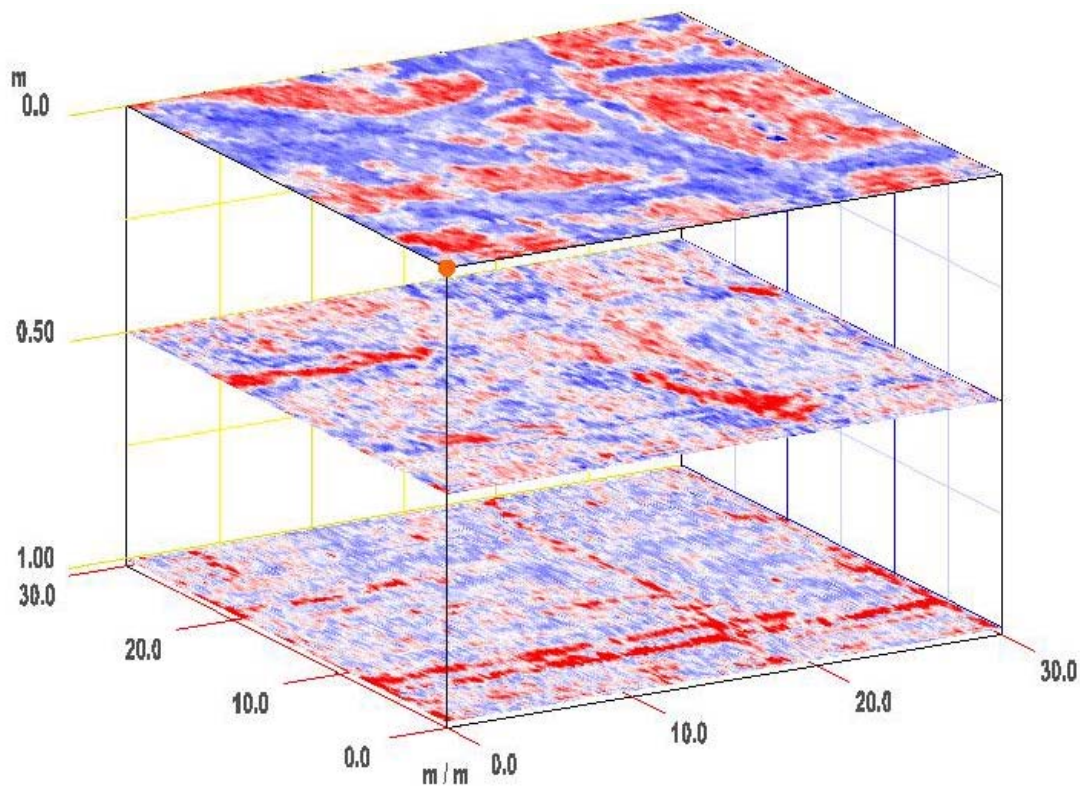


Figure 4. A set of time-slice images from Grid Site 1 showing patterns of different signal amplitudes. Assuming an average propagation velocity of 0.13 m/ns, time-slices (depth-slices) are for depths of 0, 50 and 100 cm.

Grid 2 – Jerry Brown’s buried copper tubing with antifreeze.

Jerry Brown assisted with the location of this research site and the general orientation of the buried copper tubing within the site. In this study, a 900 MHz antenna effectively outlined the area that contained the shallowly buried copper tubing.

Figure 5 is a representative radar record from Grid Site 2. On the radar record shown in Figure 5, the vertical scale is a time scale expressed in nanoseconds (ns). The horizontal scale represents units of distance and is expressed in meters. The short, white, vertical lines at the top of the radar record represent the equally-spaced (1 m), flagged reference points. In Figure 5, the upper-most continuous, high amplitude subsurface reflections (consist of three bands) represent the interface that separates the snow (A) from an organic layer (B). The bottom of the organic layer and its contact with the mineral soil is shown by a more segmented reflector that is evident between the 2.5 and 9 m distance marks. On this radar record, outside these distance marks, the organic layer is too thin to be vertically resolved with the 900 MHz antenna. The organic layer is known to be thicker in the depression under which the tubing was buried. Immediately below the organic/mineral soil interface is a zone (C) which contains a large number of point reflectors. These point reflectors represent lines of buried copper tubing, which were crossed orthogonally with the 900 MHz antenna.

Figure 6 contains a time-slice image of Grid Site 2. A 3D “cube” image of the site has been horizontally sliced at a time of 7.8 ns. Assuming a constant propagation velocity of 0.13 m/ns, a two-way pulse travel time of 7.8 ns corresponds to a depth of about 50 cm. In Figure 6, differences in color (blue and red) reveal differences in the polarity (either positive or negative) of the reflected signals. In Figure 6, the general location of the buried copper tubing has been enclosed by a polygon. A major utility line (C), which feeds the tubing system, is evident in the lower right-hand portion of this plot. Reflections and reverberations from the copper tubing (A), while correctly orientated, are highly segmented and generally unaligned. This is attributed to inadequate spatial control during surveying, irregular ground and snow surfaces, variable snow depths and soil properties, and the small diameter of the tubing (very small reflecting surface). Radar records were horizontal normalized, but the normalization distance was set by the 1 m marks on the reference line used to conduct the survey. This distance is believed to be too great for the location of 1 cm diameter, buried copper tubing. In addition, slight errors were noted in the placement of reference marks on the radar record and the actual position of the marks on the reference lines. In Figure 6, the broad area of high-amplitude reflections near “B” represents the contact of the organic with the mineral soil materials. This area (B) represents the lowest portion of the depression.

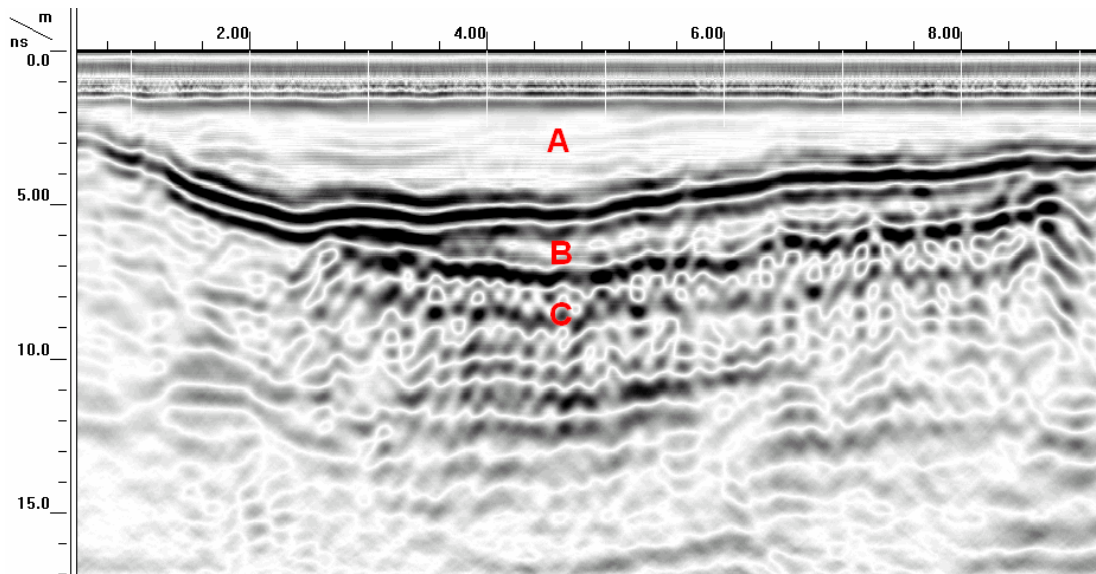


Figure 5. A representative radar record from Grid Site 2. Vertical scale is a time scale and is expressed in nanoseconds. A high-amplitude continuous reflector separates the snow (A) from an organic layer (B). Point reflectors (C) indicate the locations of the buried copper tubing.

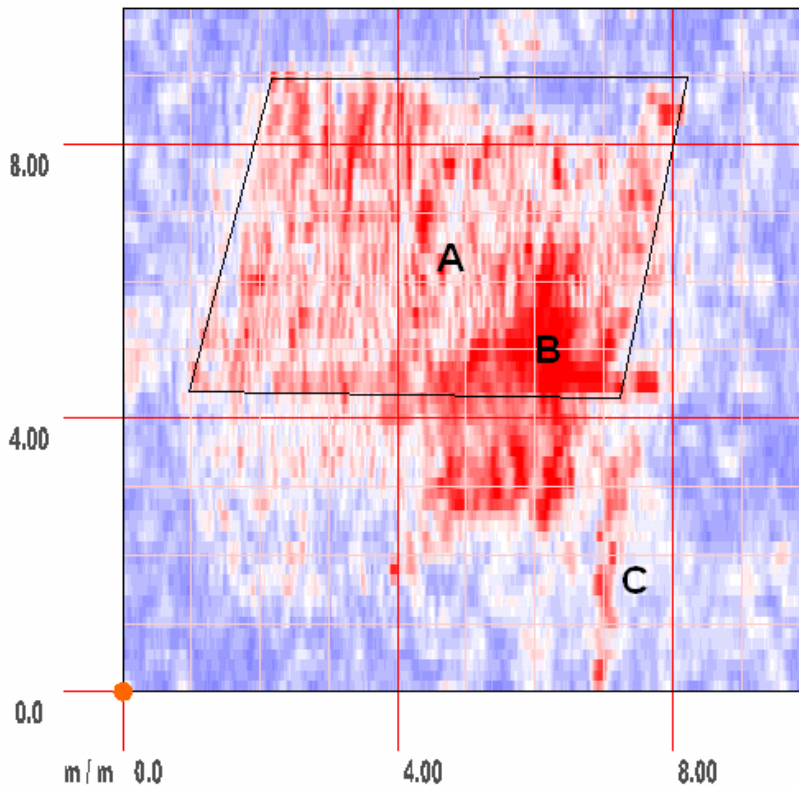


Figure 6. This time-slice image from Grid Site 2 shows the approximate locations of a main feeder pipe (C) and segments of buried copper tubing (A). The broad high-amplitude pattern near (B) represents the snow/organic mat interface. Based on a constant propagation velocity of 0.13 m/ns, this time slice (7.8 ns) is at a depth of 50 cm.

Grid Site 3:

This site is located at the southern end of a drained thaw-lake basin and contains low frost mounds. Figure 7 is a cutout cube of the 40 by 40 m grid area. In Figure 7, a 29 by 30 by 1.3 m inset has been removed from the cube display. All scales are in

meters. The vertical scale has been highly exaggerated for display purposes. The origin is located in the southeast corner of the survey area. The X axis is in the right foreground, the Y axis is in the left foreground. The depth scale assumes a constant propagation velocity of 0.13 m/ns.

All radar traverses were conducted parallel to the X axis, which is orientated in a north/south direction. As a consequence, sample traces overlap in this direction and the original signals are recovered in the data. In processing the 3D image, radar data were not continuously recorded and had to be reconstructed along the Y axis. Reconstruction was based on data recorded at points spaced 50 cm apart. As a consequence, sample traces are too widely spaced, subsurface information has been omitted, and the data is spatially aliased. Along the Y axis, radar data are interpolated by the processing algorithm between sample points spaced 50 cm apart and the resulting data appear noticeably *smudged*, less resolved, and more generalized.

In Figure 7, the base of the 1.3 m deep inset reveals linear patterns of high-amplitude reflections that have orthogonal junctions. These are interpreted as the ice-wedge networks that border ice-wedge polygons. Where these linear features intercept the vertical slices of the X and Y axes, high-amplitude vertical and horizontal reflectors are evident. These vertical and horizontal reflectors are interpreted as ice wedges. These features did not stand out and were obscured by other reflection on 2D radar records from this site. In the 3D image, these features are more prominent and meaningful.

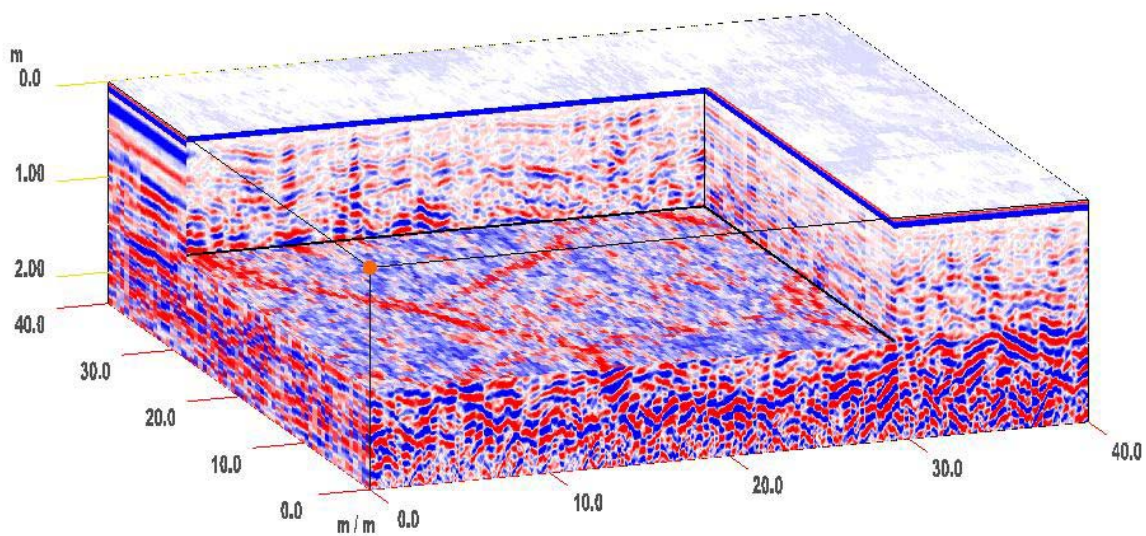


Figure 7. A 3D cube display of the Grid Site 3. A 29 by 30 by 1.3 m area has been removed from the cube display.

In Figure 7, the two horizontal bands at the top of the cube approximate the air/snow interface. As the image has not been terrain corrected, the resulting image reflects a level surface. This is incorrect, but will be accepted, as it does not necessarily weaken subsequent interpretations. In the vertical slices of the inset, the snow/soil and the organic/mineral interfaces are evident. The upper-most continuous subsurface reflector represents the snow/organic layer contact. This interface, though variable in expression appears continuous across the survey area. The slightly wavy appearance of this interface reflects the modest (5 to 50 cm) variations in snow depth measured across this site. In places, the organic materials have been disturbed by cryoturbation and mixed with mineral soil materials. Variations in signal amplitudes represent changes in ice contents of the surface layers and in the reflection coefficients of snow with ice, ice-rich organic, or ice-rich mineral soil layers.

In the upper part of the cube shown in Figure 7, interfaces are general of low to moderate amplitude and essentially horizontal or slightly inclined. These characteristics conform to layers of ice-rich organic and silty lacustrine sediments that have filled this thaw lake basin. In the lower part of the cube, interfaces are more chaotic with noticeable diffraction tails. In the lower part of the cube, signal amplitudes are generally greater indicating the presence of contrasting materials. The more chaotic reflection patterns with noticeable diffractions in the lower portion of the cube reflect the larger amounts of ice segregations and gravels. Although the radar data were migrated, hyperbolic diffractions do not appear to have been completely collapsed in this portion of the cube. These patterns are believed to be caused by ice wedges and inclined strata. The maximum depth of coring at this site was about 110 cm. Gravels were observed in some of the deeper core sections. It is possible, that the higher amplitude and more inclined interfaces in the lower part of this cube represent ice-rich, coarser-textured deposits.

Three horizontal time-slice images of Grid Site 3 are shown in Figure 8. These horizontal, time-slice images from the 3D cube have been reoriented so that the view is from directly above. For each time-slice image, the thickness of the slice was 0.19 m and the maximum reflected wave amplitude method was used. Assuming a constant velocity of 0.13 m/ns, these time slices correspond to depth slices of 0, 60, and 120 cm. On each time-slice image, a 10 m grid pattern has been superimposed.

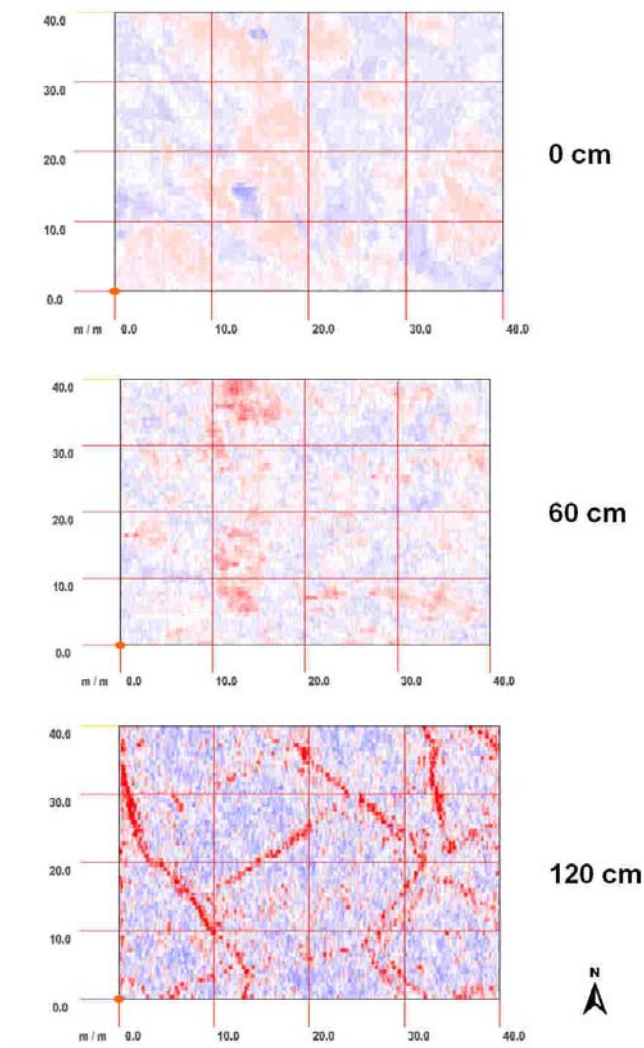


Figure 8. These three horizontal time-slice images from Grid Site 3 are from approximated depths of 0, 60, and 120 cm.

Variations in signal amplitude and polarity indicate spatial changes in soil properties. In Figure 8, in the 0 cm depth slice, areas shown in red represented higher-lying surfaces that were blanketed with a thinner snow cover. Areas shown in blue generally represented lower-lying more concave areas with thicker snow mantles. In the 60 cm slice, variations in signal amplitude and polarity are interpreted to represent interfaces within the upper part of the soil. These rather broad spatial patterns reflect, in part, variations in snow thickness, relief and soil properties, and their shared effects of propagation velocity. The ice-wedge network and the definition of ice-wedge polygons are evident in the 120 cm slice. The ice-wedge network is sufficiently contrasting in dielectric properties with the bounding permafrost (see Table 1) to provide easily identifiable, high-amplitude radar reflections. These reflections are expressed in well defined, linear patterns that intersect at various angles. Closely spaced, multiple or bifurcated patterns are evident in this slice. These linear features are well-expressed in this slice, but do not extend greatly in depth and become less distinct and quickly vanish in sequential slices. These characteristics are assumed to represent the incipient nature of the ice-wedge network that has formed in this recently drained thaw lake.

Grid Site 4.

This site is located on the Peterson Erosional Remnant. The Peterson Erosional Remnant contains numerous high centered ice-wedge polygons. Figure 9 is a cutout cube of the 30 by 30 m grid area. In Figure 9, a 24 by 24 by 1.4 m inset has been removed from the cube display. All scales are in meters. The vertical scale has been highly exaggerated for display purposes.

The grid origin is located in the northwest corner of the survey area. The X axis is in the right foreground, the Y axis is in the left foreground. The depth scale assumes a constant propagation velocity of 0.13 m/ns.

All radar traverses were conducted parallel to the X axis, which is orientated in a north/south direction. Radar imagery along these traverse lines is well resolved. However, along the Y axis, where the radar imagery has been interpolated between the equally-spaced (50 cm) traverse lines (GPR traverses were conducted orthogonal to Y axis), the data is spatially aliased.

In Figure 9, the base of the 1.4 m deep inset reveals the rather broad linear patterns of a mature ice-wedge network. The ice wedges produce generally high-amplitude reflections and have orthogonal junctions. These are interpreted as the ice-wedges that border polygons. As with the imagery from Grid Site 3, where these linear features intercept the vertical slices of the X and Y axes, high-amplitude vertical reflectors are evident. However, unlike the ice-wedge features evident at Grid Site 3, ice wedges at this site appear wider and deeper, with vertical ice-wedges better expressed on radar imagery. The ice wedge network is more intricate at this site as well. Multiple reflections suggest irregular bounding surfaces with the permafrost and possible bifurcations of individual ice wedges. In addition, in the depth-sliced or horizontal view, the segmented or broken appearance of ice wedges may be caused by the superposition and cancellation of reflected signals from these larger ground-ice masses.

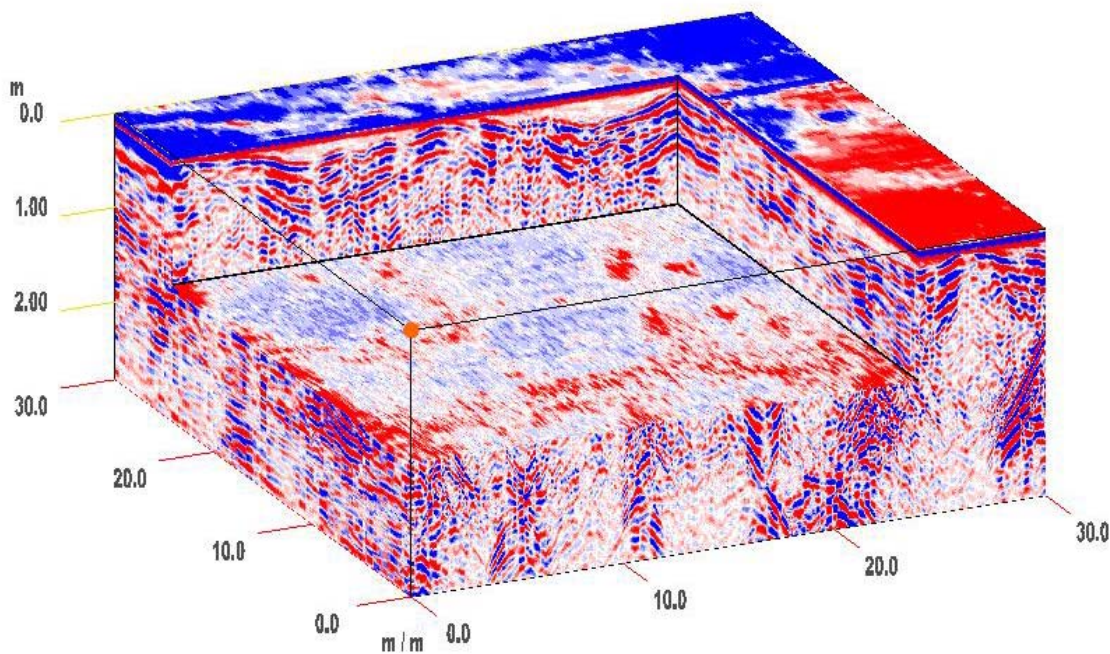


Figure 9. A 3D cube display of the Grid Site 4. A 24 by 24 by 1.4 m area has been removed from the cube display.

In Figure 9, the two horizontal bands at the top of the cube approximate the air/surface interface. As the image has not been terrain corrected, the resulting image reflects a level surface. In the upper part of the vertical slices to the inset, the snow/soil and multiple soil interfaces are evident. The upper-most continuous subsurface reflector represents the snow/soil surface contact. This interface is nearly continuous across the survey area. The wavy appearance of this interface reflects the relatively large (2 to 70 cm) differences in measured snow depth and the site's hummocky micro-topography. Variations in signal amplitude and polarity represent changes in surficial materials and in the reflection coefficients of snow with ice, ice-rich organic, or ice-rich mineral soil layers.

In the cube shown in Figure 9, reflections within the upper part of soil appear to conform to the topography of the snow/soil surface reflections. These reflections are of moderate to high amplitude, and appear fairly continuous. This seems uncharacteristic for seemingly highly-disturbed, cryoturbated soil materials. These reflections have a hummocky expression which appears to mirror the ice-wedge polygons. Subsurface reflections become more convex in appearance as they approach the soil surface on higher-lying portions of mounds. These subsurface reflections are more concave in appearance as they dip below the soil surface beneath lower-lying troughs. In general, signals appear to be more attenuated beneath the higher-lying portions of polygons. These landscape components are assumed to contain less ice, which is more transparent and less attenuating to GPR than the soil materials. Compared with the radar imagery from Grid Site 3, hyperbolic point reflectors are

more prevalent in the upper parts of soil profiles at Grid Site 4. These point reflectors form a chaotic pattern and are assumed to represent ice segregations.

In the lower part of the cube, interfaces are more chaotic. The more chaotic appearance of this portion of the cube is interpreted to reflect the presence of ice segregations. Although the radar data were migrated, hyperbolic diffractions do not appear to have been completely collapsed in this portion of the cube. These patterns are caused principally by ice wedges. Compared with the radar data from Grid Site 3 (Figure 7), reflections from ice-wedges are larger, deeper and more clearly expressed in the radar data from Grid Site 4.

Three horizontal time-slice images of Grid Site 4 are shown in Figure 10. In Figure 10, these horizontal, time-slice images from the 3D cube have been reoriented so that the view is from directly above. For each time-slice image, the thickness of the slice was 0.19 m and the maximum reflected wave amplitude method was used. Assuming a constant velocity of 0.13 m/ns, the time slices correspond to depth slices of 10, 80, and 160 cm. On each time-slice image, a 10 m grid pattern has been superimposed

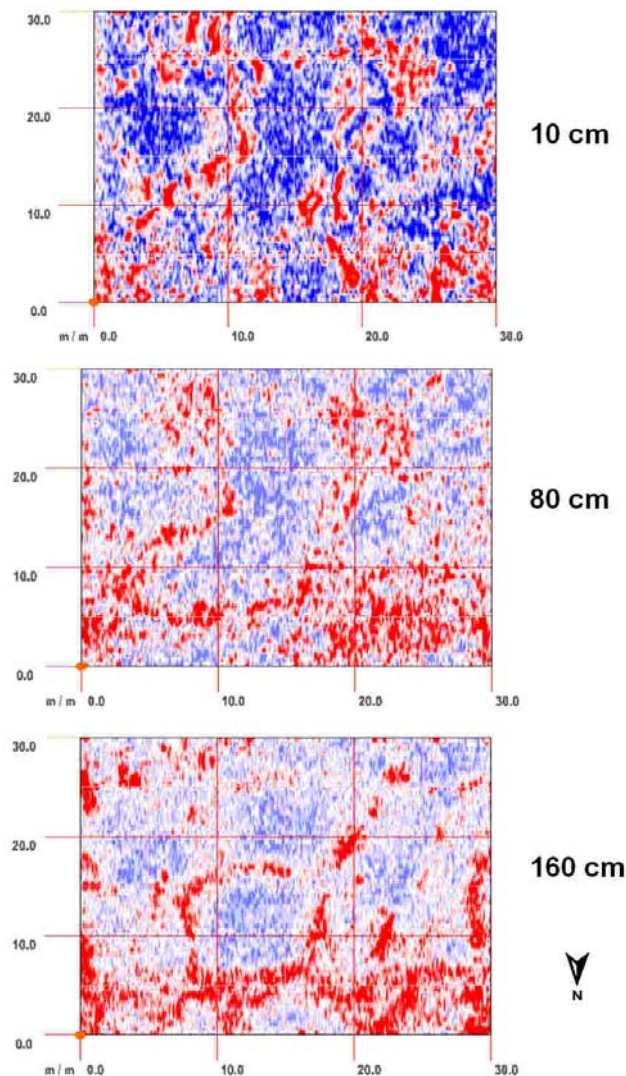


Figure 10. These three horizontal time-slice images from Grid Site 4 are from approximated depths of 10, 80, and 160 cm.

Variations in signal amplitude and polarity indicate spatial changes in soil properties. In Figure 10, in the 10 cm depth slice, areas shown in red represented the snow/ soil interface. Compare with the same interface shown in Figure 8 (from Site 3), this interface results in thin bands rather than broad, rather diffuse patterns. These characteristic suggest that the micro-topography of the two sites differs: being more irregular and hummocky at Site 4 and more level and gentler at Site 3. The segmented, curved bands seen in the 10 cm slice migrate across the grid area as the image is animated and the depth is changed. In the 80

cm slice, the arcuate bands and broad speckled patterns represent areas with higher ice contents found in troughs and flats. The ice-wedge network and the definition of ice-wedge polygons are evident in the 160 cm slice. Compared with Site 3, reflection patterns for ice wedges appear broader and deeper, but more segmented and less well defined. In this slice, these reflectors are closely spaced and suggest multiple or bifurcated ice wedge networks. These characteristics are assumed to represent radar images from a mature stage of ice-wedge development on an older surface.

References:

- Annan, A. P. and J. L. Davis. 1976. Impulse radar sounding in permafrost. *Radio Science* 2:383-394.
- Annan, A. P. and J. L. Davis. 1978. High frequency electrical methods in the detection of the freeze-thaw interface. IN: *Proceedings of the Third International Conference on Permafrost*. Edmonton, Alberta. National Research Council of Canada, Ottawa. 495-500.
- Annan, A. P., J. L. Davis, and W. J. Scott. 1975. Impulse radar wide-angle reflection and refraction sounding in permafrost. *Geological Survey of Canada Paper 75-1C*: 335-341.
- Arcone, S. A., E. F. Chacho, and A. J. Delaney. 1998. Seasonal structure of taliks beneath arctic streams determined with ground-penetrating radar. 19-24 pp. IN: Lewkowicz, A. G., and M. Allard (eds.) *Proceeding of the 7th International Conference on Permafrost*. Yellowknife, NWT, Canada, 23-27 June 1998.
- Arcone, S. A. and A. J. Delaney. 1982. Dielectric properties of thawed active layers overlying permafrost using radar at VHF. *Radio Science* 17(3): 618-626.
- Arcone, S. A. and A. J. Delaney. 1984. Radar investigations above the Trans-Alaskan Pipeline near Fairbanks. U. S. Army Cold Regions Research and Engineering Laboratory, CRREL Report 84-27.
- Arcone, S. A. and A. J. Delaney. 1989. Investigation of dielectric properties of some frozen materials using cross-borehole radiowave pulse transmission. CRREL Report 89-4.
- Arcone, S. A., P. V. Sellmann, and A. J. Delaney. 1982. Radar detection of ice wedges in Alaska. U. S. Army Cold Regions Research and Engineering Laboratory, CRREL Report 82-43.
- Asprion, U., and T. Aigner. 1997. Aquifer architecture analysis using ground-penetrating radar: Triassic and Quaternary examples (S. Germany). *Environmental Geology*, 31(1/2): 66-75.
- Asprion, U., and T. Aigner. 1999. Towards realistic aquifer models: three-dimensional georadar surveys of Quaternary gravel deltas (Singen Basin SW Germany). *Sedimentary Geology* 129: 281-297.
- Asprion, U., and T. Aigner. 2000. An initial attempt to map carbonate buildups using ground-penetrating radar: an example from Upper Jurassic SW-Germany. *Facies*, 42: 245-252.
- Beres, M., A. Green, P. Huggenberger, and H. Horstmeyer. 1995. Mapping the architecture of glaciofluvial sediments with three-dimensional georadar. *Geology*, 23(12): 1087-1090.
- Binningsbo, J., E. S. Eide, and J. F. Hjelmstad. 3D migration of GPR array-antenna data. 459-463 pp. IN: (Noon, D. editor) *Proceedings Eight International Conference on Ground-Penetrating Radar*. May 23 to 26, 2000, Goldcoast, Queensland, Australia. The University of Queensland.
- Bockheim, J. G. D. A. Walker, L. R. Everett, F. E. Nelson, and N. I. Shiklomanov. 1998. Soil and cryoturbation in moist nonacidic and acidic tundra in the Kuparuk River Basin, Arctic Alaska, U.S.A. *Arctic and Alpine Research* 30: 166-174.
- Brown, J. 1967. Tundra soils formed over ice wedges, northern Alaska. *Soil Sci. Soc. America Proc.* 31: 686-691.
- Conyers, L. B., and D. Goodman. 1997. *Ground-penetrating radar: An introduction for archaeologists*. Altamir Press, Walnut Creek, California.

- Corbeanu, R. M., G. A. McMechan, R. B. Szerbiak, and K. Soegaard. 2002. Prediction of 3-D fluid permeability and mudstone distributions from ground-penetrating radar (GPR) attributes: Example from the Cretaceous Ferron member, east-central Utah. *Geophysics* 67(5): 1495-1504.
- Corbeanu, R. M., K. Soegaard, R. B. Szerbiak, J. B. Thurmond, G. A. McMechan, D. Wang, S. Snelgrove, C. B. Forster, and A. Menitove. 2001. Detailed internal architecture of fluvial channel sandstone determined from outcrop, cores and 3-D ground-penetrating radar: Example from the middle Cretaceous Ferron sandstone, east-central Utah. *American Association of Petroleum Geologists Bulletin* 85(9): 1583-1608.
- Dallimore, S. R. and J. L. Davis. 1987. Ground-probing radar investigations of massive ground ice and near surface geology in continuous permafrost. 913-918 pp. IN: *Current Research, Part A. Geological Survey of Canada Paper 87-1A.*
- Daniels, D. J. 2004. *Ground Penetrating Radar; 2nd Edition.* The Institute of Electrical Engineers, London, United Kingdom.
- Davis, J. L., W. J. Scott, R. M. Morey, and A. P. Annan. 1976. Impulse radar experiment on permafrost near Tuktoyaktuk, Northwest Territories. *Canadian Journal of Earth Science* 13:1584-1590.
- Delaney, A. J., and Arcone, S. A. 1984. Dielectric measurements of frozen silt using time domain reflectometry. *Cold Regions Science and Technology* 9: 39-46.
- Demant, D., L. G. Evers, H. Teerlynck, B. Dost, and D. Jongmans. 2001. Geophysical investigation across the Peel boundary fault (The Netherlands) for a paleoseismological study. *Netherlands Journal of Geosciences* 80(3-4): 119-127.
- Doolittle, J. A., M. A. Hardisky, and S. Black. 1992. A ground-penetrating radar study of Goodream Palsen, Newfoundland, Canada. *Arctic and Alpine Research* 24(2):173-178.
- Doolittle, J. A., M. A. Hardisky, and M. F. Gross. 1990. A ground-penetrating radar study of active layer thicknesses in areas of moist sedge and wet sedge tundra near Bethel, Alaska, U.S.A. *Arctic and Alpine Research* 22(2): 175-182.
- Grasmueck, M. 1996. 3-D ground-penetrating radar applied to fracture imaging in gneiss. *Geophysics* 61(4): 1050-1064.
- Grasmueck, M. and A. G. Green. 1996. 3-D georadar mapping: Looking into the subsurface. *Environmental and Engineering Geoscience, Vol. II (2): 195-220.*
- Grasmueck, M., R. Weger, H. Horstmeyer. 2004. Three-dimensional ground-penetrating radar imaging of sedimentary structures, fractures, and archaeological features at submeter resolution. *Geology* (32): 933-936.
- Green, A., R. Gross, K. Holliger, H. Horstmeyer, and J. Baldwin. 2003. Results of 3-D georadar surveying and trenching the San Andreas Fault near its northern landward limit. *Tectonophysics* 368: 7-23.
- Hinkel, K. M., J. Doolittle, J. Bockheim, F. E. Nelson, R. Paetzold, J. Kimble, and R. Travis. 2001. Detection of subsurface permafrost features using ground-penetrating radar, Barrow, Alaska. *Permafrost and Periglacial Processes*. 12: 179-190.
- Hinkel, K. M., W. R. Eisner, J. G. Bockheim, F. E. Nelson, K. M. Peterson, and X. Dai. 2003. Spatial extent, age, and carbon stock in drained thaw lake basins on the Barrow Peninsula, Alaska. *Arctic, Antarctic, and Alpine Research*. 35 (3): 291-300.
- Hinkel, K. M. and F. E. Nelson. 2003. Spatial and temporal patterns of active layer depths at CALM sites in Northern Alaska, 1995-2000. *Journal of Geophysical Research-Atmospheres*, 108(D2), 10.129/2001JD000927.
- Höefle, C. M., C. L. Ping, and J. M. Kimble. 1998. Properties of permafrost soils on northern Seward Peninsula, northwest Alaska. *Soil Sci. Soc. Am. J.* 62(6): 1629-1639.
- Horvath, C. L. 1998. An evaluation of ground-penetrating radar for investigation of palsa evolution, Macmillan Pass, NWT, Canada. 473-478 pp. IN: Lewkowicz, A. G., and M. Allard (eds.) *Proceeding of the 7th International Conference on Permafrost, Yellowknife, 23 -37 June 1998.* Collection Nordicana 57. Centre d'études nordiques Université Laval, Quebec.
- Hussey, K. M. and R. W. Michelson. 1966. Tundra relief features near Point Barrow, Alaska. *Arctic* 19:162-184.

- Jol, H. M., D. C. Lawton, D. G. Smith. 2002. Ground penetrating radar: 2-D and 3-D subsurface imaging of a coastal barrier spit, Long Beach, WA, USA. *Geomorphology* 53:165-181.
- Kovacs, A. and R. M. Morey. 1979. Remote detection of massive ice in permafrost along the Alyeska pipeline and the pump station feeder gas pipeline. 268-279 pp. IN: *Proceedings of the Specialty Conference on Pipelines in Adverse Environments*. American Society of Civil Engineers. New Orleans, Louisiana, 15-17 January 1979.
- Kovacs, A. and R. M. Morey. 1985. Impulse radar sounding of frozen ground. 28-40 pp. IN: Brown, J., M. C. Metz, and P. Hoekstra (editors). *Workshop on Permafrost Geophysics*, Golden, Colorado, 23-24 October 1984. U. S. Army Cold Regions Research and Engineering Laboratory, Special Report 85-5.
- Lawson, D. E., S. A. Arcone, A. J. Delaney, J. D. Strasser, J. C. Strasser, C. R. Williams, and T. J. Hall. 1998. Geological and geophysical investigations of hydrogeology of Fort Wainwright, Alaska. U. S. Army Cold Regions Research and Engineering Laboratory, Report 98-6.
- Lehmann, F., and A. G. Green. 1999. Semiautomatic georadar data acquisition in three dimensions. *Geophysics*, 64(3): 719-731.
- Leucci, G., and S. Negri. 2006. Use of ground penetrating radar to map subsurface archaeological features in an urban area. *Journal of Archaeological Science* 33: 502-512.
- Mackay, J. R., W. H. Mathews, and R. S. MacNeish. 1961. Geology of the Engigstciak archaeological site, Yukon Territory. *Arctic* 14: 25-52.
- Mangold, N., F. Forget, F. Costard, J-Peulvast. 2005. High latitude pattern grounds on Mare: Evidence for recent melting of near-surface ground ice. *ICARUS* 174(2): 1219.pdf.
- McMechan, G. A., G. C. Gaynor, and R. B. Szerbiak. 1997. Use of ground-penetrating radar for 3-D sedimentological characterization of clastic reservoir analogs. *Geophysics*, 62(3): 786-796.
- Moorman, B. J., S. D. Robinson, and M. M. Burgess. 2003. Imaging periglacial conditions with ground-penetrating radar. *Permafrost and Periglacial Processes* 14: 319-329.
- Pilon, J. A., A. P. Annan, J. L. Davis, and J. T. Gray. 1979. Comparison of thermal and radar active layer measurements in the Leaf Bay Area, Nouveau-Quebec. *Geographie Physique et Quaternaire* 23: 317-326.
- Pilon, J. A., A. P. Annan, and J. L. Davis. 1985. Monitoring permafrost ground conditions with ground probing radar (G.P.R.) 71-73 pp. IN: Brown, J., M. C. Metz, and P. Hoekstra (editors). *Workshop on Permafrost Geophysics*, Golden, Colorado, 23-24 October 1984. U. S. Army Cold Regions Research and Engineering Laboratory, Special Report 85-5.
- Ping, C-L., M. H. Clark, and D. K. Swanson. 2004. Chapter 2. Cryosols in Alaska. 71-94 pp. IN: Kimble, J. (editor) *Cryosols-Permafrost-Affected Soils*. Springer, Verlag Berlin Heidelberg, New York.
- Price, L. W. 1972. *The Periglacial Environment, Permafrost, and Man*. Commission of College Geography, Resource Paper No. 14. Association of American Geographers, Washington, DC.
- Robinson, S. D., B. J. Moorman, A. S. Judge, and S. R. Dallimore. 1993. The characterization of massive ice at Yaya Lake, Northwest Territories using radar stratigraphy techniques. 23-32 pp. IN: *Current Research, Part B*. Geological Survey of Canada, Paper 93-1B.
- Ross, N., C. Harris, H. H. Christiansen, and B. J. Brabham. 2005. Ground penetrating radar investigations of open system pingos, Adventdalen, Svalbard. *Norwegian Journal of Geography* 59: 129-138.
- Scott, W. J., P. Sellmann, and J. A. Hunter. 1990. Geophysics in the study of permafrost. 355-384 pp. IN: *Geotechnical and Environmental Geophysics, Vol. 1: Review and Tutorial*. Society of Exploration Geophysicists Investigation in Geophysics, No. 5.
- Sellmann, P. V., J. Brown, R. I. Lewellen, H. McKim, and C. Merry. 1975. The classification and geomorphic implications of thaw lakes on the arctic coastal plain, Alaska. U.S. Army CRREL Research Report

- Sequin, M. K. 1986. Geophysics of permafrost mounds. *Eos* 67, 1401.
- Sudarmo, B., G. A. McMechan, and D. Epili. 1996. Simulation and imaging of GPR data scattered by reinforcing bars in concrete bridge deck. *Journal of Environmental and Engineering Geophysics* 1(3): 163-170.
- Szerbiak, R. B., G. A. McMechan, R. Corbeanu, C. Forster, and S. H. Snelgrove. 2001. 3-D characterization of a clastic reservoir analog: from 3-D GPR data to a 3-D fluid permeability model. *Geophysics* 66(4): 1026-1037.
- van Dam, R. L. 2002. Internal structure and development of an aeolian river dune in The Netherlands, using 3-D interpretation of ground-penetrating radar data. *Netherlands Journal of Geosciences* 81 (1): 27-37.
- Vonder Mühl, D., C. Hauck, H. Gubler. 2002. Mapping of mountain permafrost using geophysical methods. *Progress in Physical Geography* 26(4): 643-660.
- Wahrhaftig, C. 1965. Physiographic Divisions of Alaska. USGS Professional Paper 482.
- Whiting, B. M. D., McFarland, D. P., S. Hackenberger. 2000. Preliminary results of three-dimensional GPR-based study of a prehistoric site in Barbados, West Indies. 260-267 pp. IN: (Noon, D. editor) *Proceedings Eight International Conference on Ground-Penetrating Radar*. May 23 to 26, 2000, Goldcoast, Queensland, Australia. The University of Queensland.
- Wong, J., J. R. Rossiter, G. R. Olhoeft, and D. W. Strangway. 1977. Permafrost: electrical properties of the active layer in situ. *Canadian Journal of Earth Science* 14(4): 582-586.
- Wu, T., L. Shuxun, G. Cheng, and N. Zhuotong. 2005. Using ground-penetrating radar to detect permafrost degradation in the northern limit of permafrost on the Tibetan Plateau. *Cold Regions Science and Technology* 41:211-219.